PHYSICAL REVIEW E VOLUME 52, NUMBER 5 NOVEMBER 1995

Calorimetric study of chiral liquid crystals with a twist-grain-boundary phase

Tom Chan and Carl W. Garland
School of Science and Center for Material Science and Engineering, Massachusetts Institute of Technology, Cambridge, Massachusetts 02139

H. T. Nguyen
Centre de Recherche Paul Pascal, 33600 Pessac, France

(Received 19 May 1995)

High-resolution calorimetry has been used to study a homologous series of chiral liquid crystals that exhibit smectic-A (Sm-A), twist-grain-boundary (TGB_A), and cholesteric (N^*) phases. The Sm-A–TGB_A and TGB_A-N^* transitions are first order with small latent heats: 40 and 8.1 mJ/g, respectively. There is a large rounded heat capacity peak in the N^* phase that is consistent with the evolution of short-range chiral line liquid (N_L^*) character but does not represent a thermodynamic transition. All the observed features are directly analogous to those in type-II superconductors with strong fluctuations.

PACS number(s): 64.70.Md, 65.20.+w, 61.30.−v

The twist-grain-boundary (TGB) phase of a chiral liquid crystal combines a helical twist and smectic layering. The TGB_A phase was predicted theoretically by Renn and Lubensky [1] to have regularly spaced grain boundaries of screw dislocations that separate the sample into smectic-A (Sm-A) blocks, each of which is rotated about the pitch axis by a discrete amount $\Delta\theta$ relative to an adjacent block. This phase, which is an intermediate structure between Sm-A and cholesteric N^*, is the liquid-crystal analog of the Abrikosov flux vortex lattice in a type-II superconductor in an external magnetic field. The first experimental realization and characterization of the TGB_A phase was in the compounds nP1M7 (methylheptyl-alkoxyphenylpropioloyl-oxybiphenyl carboxylate) [2–5]. However, this nP1M7 series of compounds does not exhibit an N^* phase and the observed transition sequence is Sm-C^*–TGB_A–isotropic (I) [5].

The present high-resolution calorimetric study of the $n\mathrm{FBTFO_1M_7}$ homologous series [6] is aimed at elucidating the nature of the phase transitions occurring in TGB_A systems that exhibit the theoretically predicted Sm-A–TGB_A–N^* phase sequence. This work has broader implications due to the isomorphism between chiral liquid crystals and high-T_c type-II superconductors: Meissner phase ↔ Sm-A, Abrikosov vortex lattice ↔ TGB_A, Abrikosov vortex liquid ↔ a twisted chiral line liquid to be denoted as N_L^*, normal metal in a field ↔ cholesteric N^* [1,7]. The existence of significant *short-range* TGB character in the cholesteric phase, corresponding to a *liquid* of screw dislocations and deserving a new designation N_L^* to distinguish it from the usual cholesteric N^* phase [7], is supported by the results reported here.

The structural formula for $n\mathrm{FBTFO_1M_7}$ is

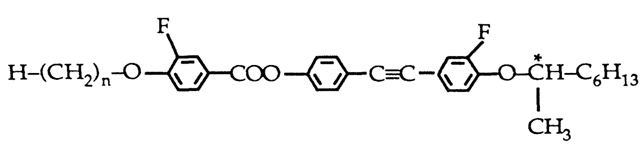

and the chemical name is 3-fluoro-4[(R) or (S)-1-methylheptyloxy] 4′-(4″-alkoxy-3″-fluorobenzoyloxy) tolan. This series of chiral molecules with a tolan core was synthesized and characterized at Centre de Recherche Paul Pascal (see Ref. [6]).

Our calorimetric results for three pure compounds ($n=9,10,11$) and one equimolar binary mixture ($n=10.5$) show that the Sm-A–TGB_A and TGB_A-N_L^* transitions are both first order with no pretransitional heat capacity C_p wings and very small latent heats L. There is no thermodynamic transition between N_L^* and N^*, which is expected theoretically since these have the same macroscopic symmetry [7] just like the situation with the vortex liquid and normal metal in type-II superconductors with strong thermal fluctuations [8]. However, a large rounded C_p peak which can be associated with the evolution of short-range TGB order is observed above the TGB_A-N_L^* transition. Furthermore, a phase diagram of n vs T, where the chain length n provides a measure of the chirality field, is topologically equivalent to the H-T phase diagram predicted for type-II superconductors with thermal fluctuations and weak quenched disorder [8].

ac calorimetric results. An overview of the heat capacity variation for $9\mathrm{FBTFO_1M_7}$ is given in Fig. 1. These data were obtained with a new high-resolution ac calorimeter [9] operating at 31.25 mHz ($\omega_0=2\pi f=0.196$), and identical C_p results were also observed at $\omega_0/9$. The qualitative features in the Sm-A–TGB_A–N^* region were the same for the other samples, as indicated by Fig. 2, where $\Delta C_p=C_p-C_p$(background) is shown for $n=9$ and 10. The quantity C_p (background) is given for $n=9$ by the dashed curve in Fig. 1. The size of the rounded N_L^*/N^* peak labeled T_5 decreases monotonically with n; ΔC_p(max) = 0.85, 0.72, 0.49, and 0.34 $\mathrm{J\,K^{-1}\,g^{-1}}$ for $n=9$, 10, 10.5, and 11, respectively. Transition temperatures for all four samples are given in Table I. It is obvious from Fig. 2 that the Sm-A–TGB_A (T_7)

1063-651X/95/52(5)/5000(4)/$06.00

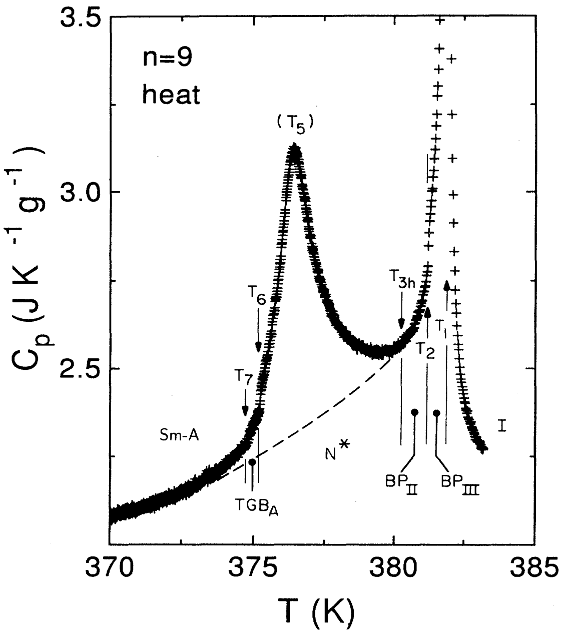

FIG. 1. Heat capacity for $9FBTFO_1M_7$ as measured at $\omega_0=0.196$ with an ac calorimeter. The dashed line represents C_p(background), the behavior expected in the N^* phase in the absence of TGB_A and Sm-A phases.

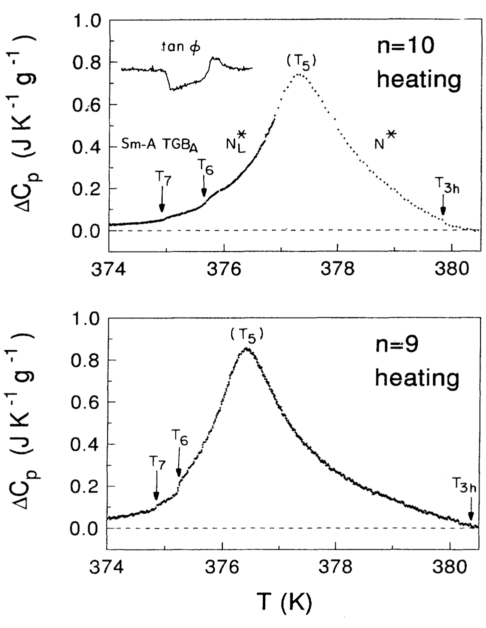

FIG. 2. Excess heat capacity $\Delta C_p = C_p - C_p$(background) for $9FBTFO_1M_7$ and $10FBTFO_1M_7$. The inset for $n=10$ shows anomalous behavior of the phase shift ϕ near the T_6 and T_7 transitions that qualitatively indicates two-phase coexistence at a first-order transition. N_L^* and N^* are *not* distinct phases but represent a cholesteric with and without short-range twisted line liquid features.

TABLE I. Transition temperatures in three nFBTFO$_1$M$_7$ chiral liquid crystals and one equimolar binary mixture. Higher temperature transitions involving isotropic and blue phase III (T_1 and T_2 in Fig. 1) have been omitted. T_5 denotes the position of a large rounded maximum in C_p in the N^* phase but does not correspond to a phase transition. Transitions T_{3c} and T_{4c} are seen *only* on cooling from the I phase, while the transition at T_{3h} occurs only on heating from temperatures below T_5.

	Transition	$n=9$	$n=10$	$n=10.5$	$n=11$
T_{3h}	N^*-BP_{II}	380.35	380.15	378.65	377.25
T_{3c}	BP_I-BP_{II}	a	379.75	378.45	376.75
T_{4c}	N^*-BP_I	377.85	378.45	377.15	375.85
T_5	(N_L^*-N^*)	376.4	377.3	376.1	374.5
T_6	TGB_A-N_L^*	375.25	375.7	373.95	373.7
T_7	Sm-A–TGB_A	374.85	375.0	373.2	–[b]

[a]The thermal anomaly at this transition was too small to detect.
[b]No Sm-A–TGB_A transition occurs for $n=11$; a Sm-C^*–TGB_A transition was observed at 370.15 K.

and TGB_A-N_L^* (T_6) transitions are difficult to detect from ac C_p data. However, the width of the TGB_A range, equal to T_6-T_7, agrees quite well with that obtained from the observation of microscopic textures [6]. Furthermore, the phase shift Φ between the oscillating T_{ac} signal and the power input $P_{ac}e^{i\omega t}$ provides a very useful qualitative indication of two-phase coexistence at a first-order transition [9]. An example of $\tan\phi \equiv \tan[\Phi+\pi/2]$ anomalies in the T_6 to T_7 region is given for $n=10$ in Fig. 2. It should be noted that hysteresis of 0.25 K was observed on heating and cooling for the phase shift anomaly associated with the Sm-A–TGB_A transition.

Nonadiabatic scanning results. Our new calorimeter is capable of fully automated operation in both ac and relaxation modes. An attractive manner of using the latter mode is to linearly ramp the heater power $P(t)$ to the sample cell while holding the bath temperature T_B constant [9]. One then obtains a quantity C_{eff} defined by

$$C_{eff}(T)=\frac{dH/dt}{dT/dt}=\frac{P-(T-T_B)/R}{dT/dt}\ , \qquad (1)$$

where R is the thermal resistance equal to the reciprocal of the thermal conductance of the link (air and lead wires) between the sample and the bath. Typical scans were taken at rates of 18 mK/min = 1 K/h (compared to 50–100 mK/h for ac calorimetry).

In the absence of two-phase coexistence, $C_{eff}(T)$ corresponds to $C_p(T)$. When a first-order coexistence of two phase occurs, C_{eff} reflects the heat effects of phase interconversion. The value of the latent heat L is then given by

$$L=\int_{T_a}^{T_b}[C_{eff}-C_p(\text{coex})]dT\ , \qquad (2)$$

where C_p(coex) is the heat capacity of the two coexisting phases $\alpha+\beta$ over a narrow coexistence range from T_a to T_b. The $C_{eff}(T)$ data for $9FBTFO_1M_7$ over the 373–378 K range are shown in Fig. 3. Superimposed on the C_{eff} data points is a smooth curve representing the C_p(ac) variation determined with the ac mode. In the coex-

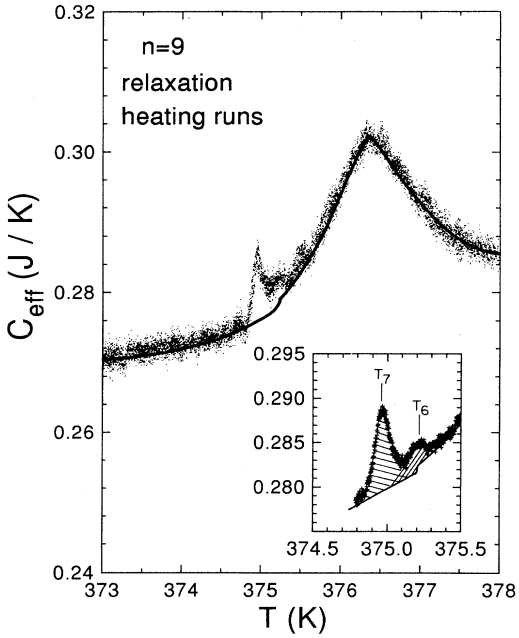

FIG. 3. $C_{eff}(T)$ data for $9FBTFO_1M_7$ obtained with the nonadiabatic scanning technique; see the text. The smooth curve represents C_p(ac) data from Fig. 1. The inset shows a detailed view of the Sm-A–TGB$_A$–N_L^* region obtained in a second run; the width of the two-phase coexistence region is ~0.3 K at T_7 and ~0.2 K at T_6. The shaded areas indicate the latent heats for a 32 mg sample.

istence region, this represents a good approximation for C_p(coex).

Note the excellent agreement between C_{eff} and C_p(ac) near the T_5 rounded peak and the clear differences observed near T_6 and T_7. These two small C_{eff} peaks reflect the latent heats L_6 and L_7 indicated by the shaded areas in the inset. It should also be noted that these nonadiabatic scanning features at T_6 and T_7 show hysteresis on heating and cooling of ~0.3 K. The data in Fig. 3 are C_{eff} and C_p(ac) values for a sample containing 32 mg of liquid crystal. The latent heat values are 0.26 mJ yielding 8.1 ± 1.2 mJ/g$=4.9\pm0.7$ J/mol for the TGB$_A$-N_L^* transition and 1.28 mJ yielding 40 ± 1.6 mJ/g$=24.2\pm1.0$ J/mol for Sm-A–TGB$_A$, where the error limits include scatter in the data and uncertainties in the choice of C_p(coex).

The small Sm-A–TGB$_A$ and TGB$_A$-N_L^* latent heats can be compared with those associated with ferroelectric-ferrielectric-antiferroelectric transitions in methylheptyloxycarbonylphenyl octyloxybiphenyl carboxylate (MHPOBC)—21.5 mJ/g=12 J/mol for Sm-C^*–Sm-C_α^*, 28.5 mJ/g=16 J/mol for Sm-C_γ^*–Sm-C^*, 16 mJ/g =9 J/mol for Sm-C_A^*–Sm-C_γ^* [10]—and the restacking transitions in the plastic crystal B phase of heptyloxybenzylidene heptylaniline (7O.7), which range from 12.5 to 38 mJ/g=5 to 15 J/mol [11].

It must be stressed that the large ΔC_p peak centered at T_5 does *not* represent a phase transition. The nonadiabatic scanning run for $n=9$ clearly shows that there are no hidden latent heat effects since the $C_{eff}(T)$ data agree very well with C_p(ac). Thus there is no first-order coexistence of two phases. The possibility of a second-order transition that is rounded by finite frequency effects due to $\omega\tau$ becoming significant compared to 1 is also extremely unlikely since the ω values are low and C_p(ac) data at 31.25 and 3.5 mHz are identical. Impurity broadening can be ruled out since other transitions, especially the I-BP$_{III}$, BP$_{III}$-BP$_{II}$, and N^*-BP$_{II}$ transitions involving blue phases, are sharp. The observed ΔC_p behavior is consistent with that expected when a twisted line liquid N_L^* (a liquid of screw dislocations of the TGB type) evolves into a chiral nematic N^* phase of the same macroscopic symmetry [7]. Naturally a structural characterization is required to identify the short-range correlations in the N_L^* region.

It should be noted that 14P1M7 exhibits a somewhat similar rounded C_p peak in the *isotropic phase* above the TGB$_A$-I transition [4,5]. The situation there is somewhat different, however, since the TGB$_A$-I latent heat is quite large. Thus any short-range TGB$_A$ character in the I phase must be quite fragmentary compared to that in N_L^*, and one must also consider the possibility of BP$_{III}$ evolution as well.

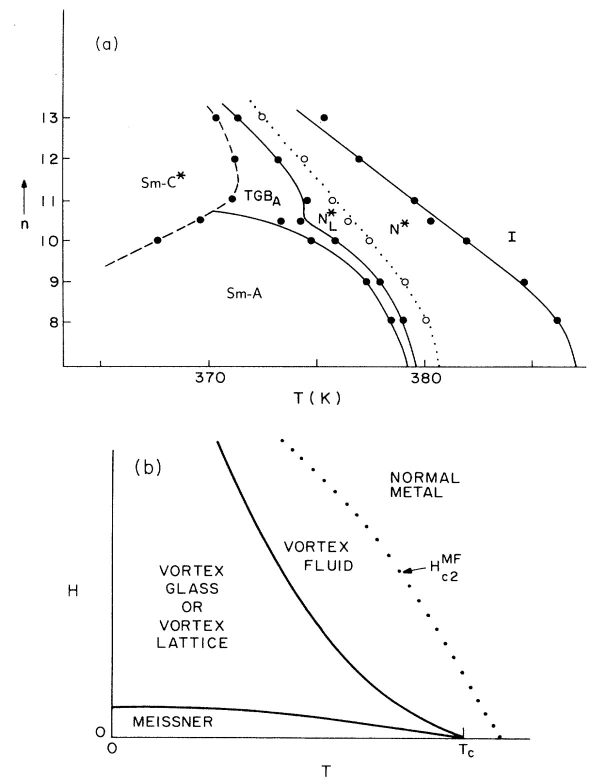

FIG. 4. (a) Phase diagram for the chiral series nFBTFO$_1$M$_7$; see text. Data for $n=8$, 12, and 13 were taken from Ref. [6]; (b) theoretical phase diagram for a type-II superconductor with strong thermal fluctuations [8]. In both cases, the dotted line is a locus of maxima in the response functions (e.g., the heat capacity), *not* a true transition line. The solid lines indicate first-order transitions, and the dashed line in (a) is a second-order transition.

Phase diagram. A plot of n vs T for the phase transitions in nFBTFO$_1$M$_7$ is given in Fig. 4(a). Data for $n=9$, 10, 10.5, and 11 come from the present study and transition temperatures for $n=8$, 12, and 13 were taken from Ref. [6]. In order to improve the clarity, all BP transitions have been suppressed. It should be noted that the length n of the alkyl and/or alkoxy end group in a series of chiral homologs is a measure of the chirality or "twist-field" strength. The usual odd-even variation in transition temperatures [6] has been eliminated by adding 2.5 K to all $n=9$ transition temperatures and 0.75 K to all $n=11$ transitions. The close correspondence between this liquid-crystal diagram and the H-T phase diagram for type-II superconductors with strong thermal fluctuations is seen by comparing Figs. 4(a) and 4(b). One cannot access zero field by varying n since $H=0$ corresponds to the absence of a twist "field." However, varying the composition of mixtures of R and S enantiomers of a strongly chiral molecule should be interesting since the racemic mixture will be nonchiral. Note that in the case of a superconductor without random pinning, a vortex liquid is expected to appear *between* the Meissner and vortex lattice phases as well as at higher temperatures, but its predicted range of stability is very narrow [8]. In the liquid-crystal system, no evidence was detected for N_L^* *between* Sm-A and TGB$_A$. However, this would be difficult to observe and it is conceivable that there is an extremely narrow range of N_L^* phase hidden in the ~ 300 mK wide coexistence region at T_7. In conclusion, the TGB$_A$-N_L^* transition at T_6, which is analogous to the melting of the Abrikosov vortex lattice, is definitely first order, a conclusion that has been reached for superconductors only on the basis of transport (resistivity) measurements, and the significant C_p peak in the N^* phase has been shown to represent a continuous evolution not accompanied by any thermodynamic transition.

The work at MIT was supported in part by the MRSEC Program of the National Science Foundation under Award No. DMR-9400334 and in part by NSF Grant No. DMR-9311853. We wish to thank T. C. Lubensky and L. Navailles for helpful discussions and H. Yao for invaluable assistance with many experimental aspects of the work.

---

[1] S. R. Renn and T. C. Lubensky, Phys. Rev. A **38**, 2132 (1988); Mol. Cryst. Liq. Cryst. **209**, 349 (1991).

[2] J. W. Goodby, M. A. Waugh, S. M. Stein, E. Chin, R. Pindak, and J. Patel, Nature (London) **337**, 449 (1989); G. Strajer, R. Pindak, M. A. Waugh, and J. W. Goodby, Phys. Rev. Lett. **64**, 1545 (1990).

[3] K. J. Ihn, A. N. Zasadzinski, R. Pindak, A. J. Slaney, and J. Goodby, Science **258**, 275 (1992).

[4] C. C. Huang, D. S. Lin, J. W. Goodby, M. A. Waugh, S. M. Stein, and E. Chin, Phys. Rev. A **40**, 4153 (1989).

[5] J. W. Goodby, I. Nishiyama, A. J. Slaney, C. J. Booth, and K. J. Toyne, Liq. Cryst. **14**, 37 (1993).

[6] A. Bouchta, H. T. Nguyen, M. F. Achard, F. Hardouin, C. Destrade, R. J. Twieg, A. Maaroufi, and N. Isaert, Liq. Cryst. **12**, 575 (1992).

[7] R. D. Kamien and T. C. Lubensky, J. Phys. (France) I **3**, 2123 (1994).

[8] D. S. Fisher, M. P. A. Fisher, and D. A. Huse, Phys. Rev. B **43**, 130 (1991), and references cited therein; D. A. Huse, M. P. A. Fisher, and D. S. Fisher, Nature (London) **358**, 553 (1992).

[9] H. Yao, T. Chan, and C. W. Garland, Phys. Rev. E **51**, 4585 (1995).

[10] K. Ema, H. Yao, I. Kawamura, T. Chan, and C. W. Garland, Phys. Rev. E **47**, 1203 (1993).

[11] J. Thoen and G. Seynhaeve, Mol. Cryst. Liq. Cryst. **127**, 229 (1985).